Model comparison for inflatables using boundary element techniques

YIC2012 — Universidade de Aveiro
First ECCOMAS Young Investigators Conference
A. Andrade-Campos, N. Lopes, R.A.F. Valente, H. Varum (editors)
24–27 April 2012, Aveiro. Portugal.

Model comparison for inflatables using boundary element techniques

T.M. van Opstal[a,⋆], E.H. van Brummelen[a]

[a] Eindhoven University of Technology,
Dept. Mechanical Engineering,
Multiscale Engineering Fluid Dynamics
PO Box 513, 5600 MB Eindhoven, the Netherlands

⋆Corresponding author: t.m.v.opstal@tue.nl

Abstract. *This paper focuses on numerical techniques for inflatable structures where, typically, the structure is a light membrane enclosing an incompressible fluid. Large displacements and subdomains with high aspect ratio are often characteristic of this class of problems, to which the finite-element/boundary-element (*FE/BE*) paradigm is an auspicious approach for numerical approximation. The* FE/BE *approach constitutes discretizing the structure with the finite-element method and employing a boundary-integral representation for the fluid problem for discretization with the boundary-element method. A marked advantage of this representation with respect to the conventional partial-differential-equation-based view of finite-element methods for fluids is the bypassing of volumetric meshing, rendering the* FE/BE *approach an enabling method for simulation of inflatables. The present work compares different structure and fluid models and judges their applicability based on numerical results.*

Keywords: Boundary-element method, fluid–structure interaction, inflatables, model comparison.

1 INTRODUCTION

Inflatable structures appear in a wide variety of engineering applications, e.g., evacuation slides in aircraft, air beams for temporary civil structures, stowable space structures and air cushions. One of the most prominent examples of an inflatable structure is the airbag. Often, these inflatable structures are stowed in highly-complex folded configurations and, moreover, undergo large displacements during their deployment. Commonly, in computational fluid dynamics a partial differential equation (PDE) governs the flow on the internal domain and numerical approximation of this flow involves generating a mesh on this domain that should evolve with the structural motion. For realistic stowed airbags, existing meshing procedures are far from generating a mesh robustly on the highly complex initial geometry. Volumetric remeshing strategies furthermore fall short in maintaining sufficient regularity and resolution for reliable predictions at a reasonable computational cost.

There is, therefore, a need for approximations to fluid response that bypass volume meshing. In industry, within the context of airbag modeling, this is done by assuming a predefined (usually uniform) pressure distribution on the structure. This approach however fails when a detailed understanding of the dynamics is required [9]. Inside the folded geometry, the flow can however be assumed to be of a simple (viz. linear) nature. This pivotal assumption allows for an equivalent boundary-integral representation of the fluid. This, in turn, renders the coupled system of equations amenable to a FE/BE [3, 5, 15] approach in which both the fluid and structure are cast into variational forms with the fluid–structure interface as domain, thus avoiding all computations on the deforming internal domain.

To gain understanding and judge the viability of the methodology, we first assess the FE/BE paradigm in a two-dimensional setting. This work addresses modeling aspects and provides relatively simple computations to compare different fluid and structure models. More advanced computations are deferred to [12, 13] in this work. Two alternate structure models are derived. Also, the boundary-integral formulation of a hierarchy of three common fluid models (viz. uniform pressure, potential flow and Stokes flow) are discussed. The setup of the remainder of this paper is presented after the problem statement in §1.1.

1.1 Problem statement

We introduce some notation and definitions to facilitate the subsequent discussion of the model. The symbol $\boldsymbol{x}$ is simultaneously identified with a function and the value it attains at a particular point. We resort to index notation (x_i) when confusion may otherwise arise. The L^2 inner product is denoted $(\boldsymbol{a}, \boldsymbol{b})_{L^2(S)} = \int_S a_i b_i$. The Lebesgue measure of a space S is denoted $m(S)$, and $|\cdot|$ denotes the Euclidean norm.

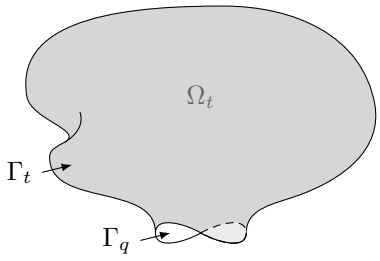

Figure 1: Schematic geometry of inflatable structure.

To fix thoughts, consider a thin, flexible structure enclosing a linear, incompressible fluid as shown in figure 1. The structure is assumed to be a $d-1$ dimensional surface in $\mathbb{R}^d$, which, for some time $t \in (0, T)$, can be related to some parameterization $\boldsymbol{\theta}$ through the mapping $(\boldsymbol{\theta}, t) \mapsto \boldsymbol{x} \in \Gamma_t$. The boundary $\partial\Omega_t$ of the fluid domain Ω_t comprizes an inflow boundary Γ_q, and a wet boundary Γ_t, which it shares with the structure. When no confusion arises, we sometimes suppress the subscript t. The dimension of the problem is d, where $d = 3$ corresponds to the physical case and $d = 2$ to the sought after planar environment in which we assess the FE/BE paradigm. Throughout, we consider a space $\mathbb{V}$ of sufficiently smooth mappings $S \times (0, T) \to \mathbb{R}^d$ satisfying the initial- and boundary conditions, inside which we seek a structural response $\boldsymbol{x}$. We test against $\mathbb{V}_0$, constructed as $\mathbb{V}$, but with homogeneous initial- and boundary conditions. The aggregated fluid-structure interaction problem can then be condensed into the following variational formulation:
find $\boldsymbol{x}, \lambda \in \mathbb{V} \times \mathbb{R}$ *s.t.* $\forall \boldsymbol{w}, \mu \in \mathbb{V}_0 \times \mathbb{R}$:

$$(\varrho_0 \boldsymbol{x}', \boldsymbol{w}')_{L^2(S)} - a(\boldsymbol{x}; \boldsymbol{w}) + (\boldsymbol{t}(\boldsymbol{x}), \boldsymbol{w})_{L^2(S)} + \mu V(\boldsymbol{x}, t) + \lambda \langle \delta_{\boldsymbol{x}} V(\boldsymbol{x}, t), \boldsymbol{w} \rangle = \boldsymbol{0}. \tag{1}$$

We consider the terms of this variational statement term-wise:

1. The inertia term, in which ϱ_0, the fabric density, is henceforth assumed unity for simplicity;
2. The stiffness semilinear form, $a(\cdot;\cdot)$, for which two choices are derived in section 2;
3. The fluid load, the fluid being interpreted as a Steklov-Poincaré operator assigning to each $\boldsymbol{x}$ a traction $\boldsymbol{t}$. In section 3 a hierarchy of fluid models is proposed for which $\boldsymbol{t}$ is explicitly derived;

4&5. Terms ensuring that fluid incompressibility is respected. The first of these is the volume constraint (cf. §3.1), and the second its Fréchet derivative with respect to $\boldsymbol{x}$.

After the introduction of the models, section 4 proceeds with a comparison by means of a prototypical inflation problem, viz., the inflation of the pancake-shaped domain. On the basis of these simulations, we draw conclusions in section 5.

2 STRUCTURE MODELS

Inherently, our final interest goes out to problems set in $d = 3$. Two competing views can be entertained in deriving an "equivalent structural response" in $d = 2$, by this we mean that the same qualitative behavior is present, concerning internal forces. The main force present is the membrane (or in-plane) force, this behavior needs to be retained. In addition, flexural rigidity is observed to be an important component of the model. Physically, a fold in the fabric will resist total flattening due to the small amount of bending stiffness present. Numerically, we observe that the stability of the model with only membrane contributions is severely reduced due to degeneracy. The small bending contribution can thus be seen as a regularization. Finally, from the point of view of analysis, the introduced extra regularity aids the establishment of bounds to the response. These motivations are elaborated upon in [12]. Concerning the two competing views, we first derive, in §2.1, the internal forces of a univariate string directly from

three-dimensional elasticity and restrict the response to a plane. Alternatively, we can assume a bivariate description of a fabric and consider the case where the response is constant perpendicular to our plane of interest, see §2.2. In both cases we assume a linearly elastic response. In §2.3 we study the obtained constitutive relations from a physical point of view and provide a qualitative comparison.

2.1 String Model

One departure point for a mathematical model of the airbag fabric, is the well-known equation of three-dimensional elastodynamics. Consider an initial material domain ω_0 and an evolving position field $\boldsymbol{x} : \omega_0 \times (0,T) \longrightarrow \mathbb{R}^3$. Define the current domain as $\omega_t := \boldsymbol{x}(\omega_0, t)$. The load due to internal stress, is given in Lagrangian form by

$$x_i \mapsto -\frac{\partial}{\partial \chi_i}(F_{ij}S_{jk}), \tag{2}$$

see e.g. [10]. In this equation, $F_{ij} := \partial x_i/\partial \chi_j$ is the deformation gradient and S_{ij} is known as the 2nd Piola-Kirchhoff stress tensor. The constitutive relation $\boldsymbol{S}(\boldsymbol{F})$ is commonly derived from a potential energy functional $\boldsymbol{x} \mapsto \Psi(\boldsymbol{x}) \in \mathbb{R}_{\geq 0}$, as $\boldsymbol{S} := \delta_{\boldsymbol{E}}\Psi$ with $\boldsymbol{E} := (\boldsymbol{F}^T\boldsymbol{F} - \boldsymbol{I})/2$ the Green-Lagrange strain tensor. We now introduce the underlying assumptions for the planar membrane problem under consideration:

1. The three-dimensional body has a string-like shape with a small circumference. Introduce a univariate parameterization $s \mapsto \boldsymbol{\chi}(s)$ which maps S onto a centerline $\Gamma_0 \in \omega_0$. The tangential direction can then be defined as $\boldsymbol{\tau} := (d\boldsymbol{\chi}/ds)|d\boldsymbol{\chi}/ds|^{-1}$. Then, we can postulate the strains perpendicular to this tangent to be negligible;
2. This parameterization is sufficiently smooth; and
3. We restrict the response to the plane, $\mathbb{R}^2$.

We choose the arc-length parameterization, such that $|D\boldsymbol{\chi}| = 1$, and recall that the material under consideration is taken linearly elastic, thus $2\Psi := \hat{c}(|D\boldsymbol{x}| - 1)^2$ (see [14]), with constant $\hat{c} > 0$. It now follows that $\mathrm{grad}_{\boldsymbol{\chi}} = D$, $\boldsymbol{F} = D\boldsymbol{x}$ and $\boldsymbol{S} = \delta_a\Psi(\delta_a E)^{-1} = \hat{c}(1 - |D\boldsymbol{x}|^{-1})$ where we have abbreviated $|D\boldsymbol{x}|^2 = a$. We also add flexural regularization controlled by $1 \gg \hat{d} > 0$ of the form $\hat{d}|D^2\boldsymbol{x}|^2$. This yields, for (2),

$$\boldsymbol{x} \mapsto -D(D\boldsymbol{x}\hat{c}(1 - |D\boldsymbol{x}|^{-1})) + D^2(\hat{d}D^2\boldsymbol{x})$$

and the *string* semilinear form $a_\varsigma(\boldsymbol{x}, \boldsymbol{w}) := \hat{c}([1 - |D\boldsymbol{x}|^{-1}]D\boldsymbol{x}, D\boldsymbol{w})_{L^2(S)} + \hat{d}(D^2\boldsymbol{x}, D^2\boldsymbol{w})_{L^2(S)}$. We note that this variational form can also be derived by reversing the steps of setting up a force balance and chosing a parameterization, as is done in [1, 14].

2.2 Kirchhoff-Love Model

In $d = 3$, the Kirchhoff-Love (K-L) shell is a commonly used fabric model (e.g. [4]) and provides an alternate starting point for deriving an equivalent univariate structure model in $d = 2$. An introduction to this model can be found in, for instance, reference [2]. In the following discussion, we assume knowledge of the basics of K-L shell theory as elaborated upon in this reference. A parameterization $\boldsymbol{\theta}$ of $S \subset \mathbb{R}^2$ is chosen, together with a reference configuration $\boldsymbol{\chi}(\boldsymbol{\theta})$ and a current configuration $\boldsymbol{x}(\boldsymbol{\theta}, t)$. The cornerstone assumption to arrive at the planar model is that the solution is constant in the out-of-plane direction. Aligning the coordinate system appropriately (i.e. defining both θ_2, χ_3 and x_3 perpendicular to the chosen plane) we can formulate this assumption as

$$x_3 = 0, \ \frac{\partial x_i}{\partial \theta_2} := x_{i,2} = \delta_{i-3}, \tag{3}$$

respectively, in which indices behind the comma denote derivatives w.r.t. the corresponding parametric coordinate. In K-L theory, the potential energy takes the form [2]

$$a_k(x) = \frac{1}{2}\int_S H^{\alpha\beta\gamma\delta}(c\varepsilon_{\alpha\beta}\varepsilon_{\gamma\delta} + d\kappa_{\alpha\beta}\kappa_{\gamma\delta}),$$

where $H^{\alpha\beta\gamma\delta} := \eta a^{\alpha\beta}(\boldsymbol{\chi})a^{\gamma\delta}(\boldsymbol{\chi}) + \frac{1}{2}(1-\eta)(a^{\alpha\gamma}(\boldsymbol{\chi})a^{\beta\delta}(\boldsymbol{\chi}) + a^{\alpha\delta}(\boldsymbol{\chi})a^{\beta\gamma}(\boldsymbol{\chi}))$ is the constitutive tensor, $\varepsilon_{\alpha\beta}$, $\kappa_{\alpha\beta}$ are the strain and bending strain, c and d are scalar constants and η is Poisson's ratio. We proceed by reducing the building blocks of the K-L potential energy. The jacobian becomes $\boldsymbol{x}_{,\alpha} = \boldsymbol{x}_{,1} =: D\boldsymbol{x}$; the 1st fundamental form,

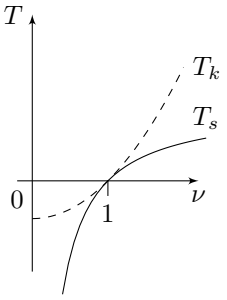

Figure 2: Constitutive relation as proposed by [14] (solid) and as derived from K-L (dashed).

$a_{\alpha\beta}(\boldsymbol{x}) := x_{i,\alpha}x_{i,\beta} = x_{1,1}^2 + x_{2,1}^2 = |D\boldsymbol{x}|^2$; the contravariant metric tensor, $a^{\alpha\beta}(\boldsymbol{x}) = [a_{\alpha\beta}]^{-1} = |D\boldsymbol{x}|^{-2}$; the normal, $n_i := \boldsymbol{x}_{,1} \times \boldsymbol{x}_{,2}/|\boldsymbol{x}_{,1} \times \boldsymbol{x}_{,2}| = \{x_{1,1}, x_{2,1}, 0\} \times \{0,0,1\}/|\{x_{1,1}, x_{2,1}, 0\} \times \{0,0,1\}| =: \text{rot}_{ij}Dx_j/|D\boldsymbol{x}|$; and the 2nd fundamental form, $b_{\alpha\beta} := -x_{i,\alpha\beta}n_i = -n_iD^2x_i$.
We chose a flat, unstretched reference configuration $\boldsymbol{\chi}$, such that $|D\boldsymbol{\chi}| = 1$ and $|D^2\boldsymbol{\chi}| = 0$. Strain then reduces to $\varepsilon_{\alpha\beta} = x_{i,\alpha}x_{i,\beta} - \chi_{i,\alpha}\chi_{i,\beta} = |D\boldsymbol{x}|^2 - 1$; and bending strain to $\kappa_{\alpha\beta} = -x_{i,\alpha\beta}n_i + \chi_{i,\alpha\beta}n_i(\chi) = -n_iD^2x_i$. Introducing these building-blocks into the potential energy above yields

$$a_k(x) = \frac{1}{2}\int_0^L \hat{c}(|D\boldsymbol{x}|^2 - 1)^2 + \hat{d}|n_iD^2x_i|^2$$

where

$$\hat{c} := \overbrace{|D\boldsymbol{\chi}|^{-4}}^{=1}\frac{1}{2}\frac{Eh}{1-\eta^2}, \qquad \hat{d} := \frac{\hat{c}h^2}{12},$$

E is Young's modulus and h the membrane thickness. The bending term serves as a regularization and should not be the dominant behavior, as explained at the beginning of this section. We assume that for regularization purposes a linear approximation of this term suffices. Considering the decomposition $|D^2\boldsymbol{x}| = |n_iD^2x_i| + |t_iD^2x_i|$, we assume the last term to be negligible. Inserting this linear approximation into the energy functional and finally taking the Gâteaux derivative, yields the desired form

$$a_k(\boldsymbol{x};\boldsymbol{w}) := \langle \delta_{\boldsymbol{x}}a_k(\boldsymbol{x}), \boldsymbol{w}\rangle = \int_S \hat{c}(|D\boldsymbol{x}|^2 - 1)Dx_iDw_i + \hat{d}D^2x_iD^2w_i. \tag{4}$$

2.3 Physical interpretation

We now compare the plane strain components of the stored energies of the above two derivations. Labeling the stretch $|Dx| =: \nu \in (0,\infty)$, the (magnitude of the) tension force in section 2.2, according to equation (4) reads $T_k(\nu)/\hat{c} := \nu^2 - 1$. This is different from the tension in section 2.1, $T_s(\nu)/\hat{c} = 1 - \nu^{-1}$. For a graphical comparison, cf. figure 2. Both constitutive relationships can however be classified as *elastic*, as they depend only on the stretch. From a physical standpoint, $T(\nu)$ should satisfy the following requirements [1, §2.2]:

1. strictly increasing. $(T(\nu_2) - T(\nu_1))(\nu_2 - \nu_1) \geq 0$ with equality if and only if $\nu_1 = \nu_2$
2. *natural* reference configuration. $T(1) = 0$
3. tensile limit. $T(\nu) \to \infty$ as $\nu \to \infty$
4. compressive limit. $T(\nu) \to -\infty$ as $\nu \to 0$

We note that T_s and T_k violate the requirement on the tensile and compressive limits respectively. However, in view of the application we anticipate small strains ($|\nu - 1| \ll 1$). It is also in this regime that the response is seen to be identical up to quadratic terms.

3 FLUID MODELS

The second modeling decision in the force balance (1) is that of the fluid response to a structural configuration $\boldsymbol{x}$. We consider the enclosed fluid to be incompressible, and a prescribed inflow to be given. Traditionally, the assumption

of a uniform pressure has been employed to bypass the need for a volume mesh, see §3.1. This, however, provides an inadequate approximation of the fluid behavior to capture the inflation dynamics. We will observe this in the numerical experiments conducted in §4.2. Owing to the FE/BE approach, better approximations can be made without resorting to a volumetric mesh. We present the potential flow model in §3.2 and the Stokes flow model in §3.3. Uniform pressure, potential flow and Stokes flow provide a hierarchy of models, in the sense that they can be derived from the incompressible Navier-Stokes equations (e.g. [7]), under decreasingly restrictive assumptions.

3.1 Uniform pressure

The simplest conceivable fluid model is a uniform pressure on Γ_t. This model is popular in applications as it bypasses the computation of a fluid approximation on the intricately folded domain. The pressure is determined based on the instantaneous volume of the airbag and injected mass, through a gas law. In [12] it is demonstrated that, for incompressible flows, the uniform pressure level corresponds to the Lagrange multiplier pertaining to the volume constraint $V(\boldsymbol{x},t)=0$. In particular, with reference to equation (1), the volume constraint is defined as

$$V(\boldsymbol{x},t) := m(\Omega_t) - v(t) = 0, \qquad v(t) := m(\Omega_0) - \int_0^t \int_{\Gamma_q} q,$$

where the $\boldsymbol{x}$-dependence stems from the definition of Ω_t through its boundary $\Gamma_t = \boldsymbol{x}(S,t)$, v is the predefined evolution of the volume following from the sum of the initial volume and $q : \Gamma_q \times (0,T) \mapsto \mathbb{R}$, a predefined outflux. The pressure level then corresponds to λ. The uniform-pressure model provides a trivial approximation for the traction in equation (1):

$$\boldsymbol{t}_u := \boldsymbol{0} \tag{5}$$

Hence, the fluid modeling is indeed entirely bypassed.

3.2 Potential flow

Considering quasi-stationary, irrotational flow, the velocity can be expressed as the gradient of a velocity potential ϕ. The fluid response is then entirely determined by incompressibility. According to the kinematic condition of fluid–structure interaction (FSI), the normal velocity of the fluid on the interface coincides with to the normal velocity of the structure. This condition is also called the slip condition. The Laplace-Neumann problem results:

$$\begin{cases} -\Delta\phi = 0, & \text{on } \Omega, \\ \partial_{\boldsymbol{n}}\phi = \boldsymbol{n}\cdot\boldsymbol{x}' & \text{at } \partial\Omega. \end{cases}$$

Boundary integral theory provides a reformulation of this problem set on the boundary [11]. We give here the direct formulation

$$c\phi + K_p\phi = V_p(\boldsymbol{n}\cdot\boldsymbol{x}'),$$

where

$$V_p\phi := -\frac{1}{2\pi}\oint_{\partial\Omega}(\log r)\phi(\boldsymbol{y})dm_{\boldsymbol{y}}, \qquad K_p\psi := -\frac{1}{2\pi}\oint_{\partial\Omega}\frac{(\boldsymbol{x}-\boldsymbol{y})\cdot\boldsymbol{n}(\boldsymbol{y})}{r^2}\psi(\boldsymbol{y})dm_{\boldsymbol{y}}$$

denote convolutions, the subscript p stressing the fact that the associated kernels are related to potential flow. Also, $r=|\boldsymbol{x}-\boldsymbol{y}|$ and c is a constant related to the geometry of the boundary, in the case of a smooth boundary, $c=1/2$. The weak form, on which the discretization is based, is obtained through an inner product with a test function w:

$$\big(w,(1/2+K_p)\phi\big)_{L^2(\partial\Omega)} = \big(w,V_p(\boldsymbol{n}\cdot\boldsymbol{x}')\big)_{L^2(\partial\Omega)},$$

where we remark that the inner products are to be interpreted in the distributional sense. The traction acting on the interface are determined by the potential through the well-known Bernoulli relation:

$$\boldsymbol{t}_p := -\frac{1}{2}\rho|\nabla\phi(\boldsymbol{x})|^2, \tag{6}$$

where ρ is the fluid density and ∇ the spatial gradient. Because of the quasi-stationarity assumption the term ϕ' is disregarded. This would lead to significantly increasing complexity pertaining to extending ϕ, as we consider a time-dependent fluid domain. The present discussion is a concise derivation. For more details cf. [12].

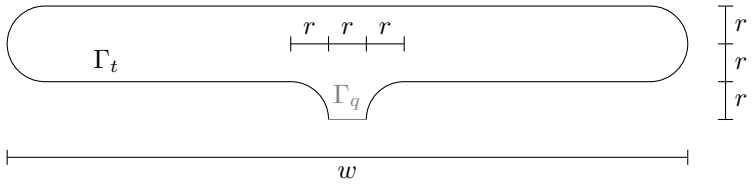

Figure 3: Pancake-shaped domain, initial geometry.

3.3 Stokes flow

In the case of viscosity-dominated flow, we drop the irrotationality assumption, and arrive at the Stokes equation set on Ω. The kinematic condition at $\partial\Omega$ now engenders a Dirichlet condition on the fluid velocity.

$$\begin{cases} \sigma_{ij,j} = 0, & \text{in } \Omega, \\ u_{i,i} = 0, & \text{in } \Omega, \\ u_i = x_i' & \text{at } \partial\Omega. \end{cases}$$

with stress $\sigma_{ij} = \delta_{i-j}p - \mu(u_{i,j} + u_{j,i})$, $t_i = \sigma_{ij}n_j$, pressure p, velocity u_i and viscosity μ. Note that, as opposed to the potential flow model, both components of the velocity field are specified in the Stokes model, not only the normal component. This kinematic condition is also called the no-slip condition. Again, a boundary integral representation is available [8]. We present the direct formulation, which yields an implicit form of the sought-after Steklov-Poincaré map. The according weak form reads:

$$\left(w_k, (\delta_{i-k}/2 + [K_s]_i^k)x_i'\right)_{L^2(\partial\Omega)} = \left(w_k, [V_s]_i^k[-t_s]_i\right)_{L^2(\partial\Omega)}, \tag{7}$$

where

$$[V_s]_i^k u_i := \frac{1}{4\pi\mu}\oint_{\partial\Omega}\left(-\delta_{i-k}\log r + \frac{(x_i - y_i)(x_k - y_k)}{r^2}\right)u_i(\boldsymbol{y})dm_{\boldsymbol{y}},$$
$$[K_s]_i^k t_i := \frac{1}{\pi}\oint_{\partial\Omega}\frac{(x_i - y_i)(x_k - y_k)(x_j - y_j)n_j}{r^4}t_i(\boldsymbol{y})dm_{\boldsymbol{y}}$$

The minus sign before $\boldsymbol{t}_s$ arises from considering the tractions acting on the structure, i.e., the reaction force. For a more detailed discussion, cf. [13].

4 NUMERICAL EXPERIMENTS

We study the structure and fluid models of the previous two sections and apply them to the pancake inflation model problem. The initial configuration is as given in figure 3 with geometrical parameters $r = 1/3, w = 9$. We set the string rigidity to $\hat{c} = 1$ and the flexural rigidity to $\hat{d} = 1 \cdot 10^{-6}$. Moreover, we set the fluid density to $\rho = 1$ and, in the case of Stokes flow, the viscosity to $\mu = 5 \cdot 10^{-3}$. The inflow is specified as $q = \overline{q}\sigma(s)\theta(t)$, with

$$\sigma(s) = 4s(r - s)/r^2$$
$$\theta(t) = \frac{1}{t_2}\begin{cases} (1 - \cos(\pi t/t_1))/2, & 0 < t \le t_1, \\ 1, & t_1 < t \le t_2, \\ (1 + \cos(\pi(t - t_2)/t_1))/2, & t_2 < t \le t_1 + t_2, \\ 0, & t_1 + t_2 < t < T. \end{cases}$$

In these relations we have $t_1 = 100$, $t_2 = 200$, $T = 500$ and the mean influx $\overline{q} = (m(\Omega_0) - m(\Omega_T))/t_2$. The final volume corresponds to that of a circle with a 5% larger circumference as the initial configuration. Note that the mean flux has a negative sign as it is directed into the enclosure.

The parametric domain S is divided into 64 elements and the time step is 0.44. The structure weak form (1) is discretized using $H^2(S)$-conforming Hermite elements [6] and the resulting nonlinear system solved iteratively with Newton's method. The solution $\boldsymbol{x}(\cdot, t)$ is projected (in the $L^2(S)$ sense) onto a linear basis in which the isoparametric discretization of the fluid problem is set. This linear description enables easy analytic evaluation of the singular integrals. Within a time-level we subcycle between the structure and fluid solvers in a partitioned

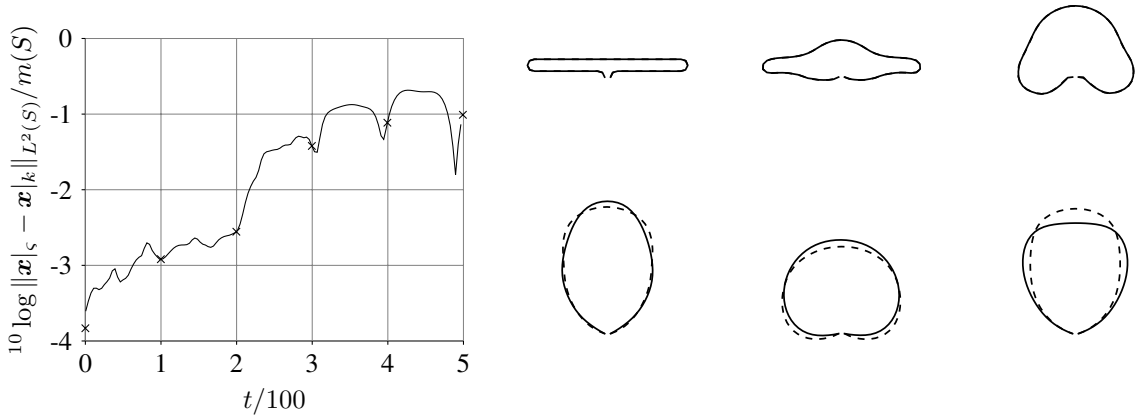

Figure 4: Left panel: time evolution of the difference between the structural response measured in the $L^2(S)$ norm. Right panel: snapshots of the response at the $\times$-marked time levels, $\boldsymbol{x}|_k$ (solid), $\boldsymbol{x}|_\varsigma$ (dashed).

manner until convergence is reached. A simple backward Euler time-integration scheme is used for the temporal discretization and provides the required numerical damping. We note that the Petrov-Galerkin interpretation of this scheme utilizes a linear trial space and a piece-wise constant test space.

In the following, the responses are compared in the L^2 norm, always dividing by $m(S)$. We denote the response using model a by $\boldsymbol{x}|_a$, where $a \in \{k, \varsigma, u, p, s\}$ denotes the *k*irchhoff-love-based, *s*tring, *u*niform pressure, *p*otential flow and *s*tokes flow models respectively.

4.1 Comparison of structural models

The response for the different structural models is studied in combination with Stokes flow. The right panel of figure 4 displays snapshots of both structural responses. First, we observe an inflation phase and, ensuing, a periodic "breathing motion", in which the system oscillates due to the momentum supplied by the inflow and reactive forces at the hinged supports. This motion is damped out slowly due to dissipation in the fluid and numerical dissipation in the time integration and in the limit $T \to \infty$ will assume its steady position. The left panel of this figure shows that the difference between the solutions jumps to $\mathcal{O}(10^{-4})$ immediately, due to strains introduced when constructing the initial configuration. As the initial configuration is constructed similarly in all numerical experiments, this same phenomenon is observed throughout the present section. The introduced spurious strains decay under mesh refinement. The difference accumulates initially during the inflation period, remaining high during the breathing motion, and decreasing as the system tends to its steady inflated position. The responses remain identical, quantitatively speaking, as is seen in the right panel of figure 4, and the relative errors pertain mainly due to the out-of-phase breathing motion.

We also consider the behavior as time tends to infinity, see figure 5. The left panel show the linear decay of the difference in L^2 sense of the responses for the two structure models, the right panel shows that the steady state response is almost identical. The L^2 difference for this plot is less than 10^{-6}.

4.2 Comparison of fluid models

The hierarchy of fluid models are compared using the string model for the structure. Again we give the evolution of the differences in the L^2 norm, and snapshots of the response. In figure 6 we see that the uniform pressure model and potential flow model produce almost identically the same initial inflation response, and qualitatively the same response throughout the simulation. Stokes flow gives a qualitatively different response from the onset, due to the added modeling of viscosity.

To see that this trend is more marked as the complexity of the problem increases, the experiment is repeated with $w = 20$, corresponding to an aspect ratio of 30. This case has been selected to increase complexity while avoiding self contact, which is not treated in the uniform pressure model. In addition we have divided the domain into

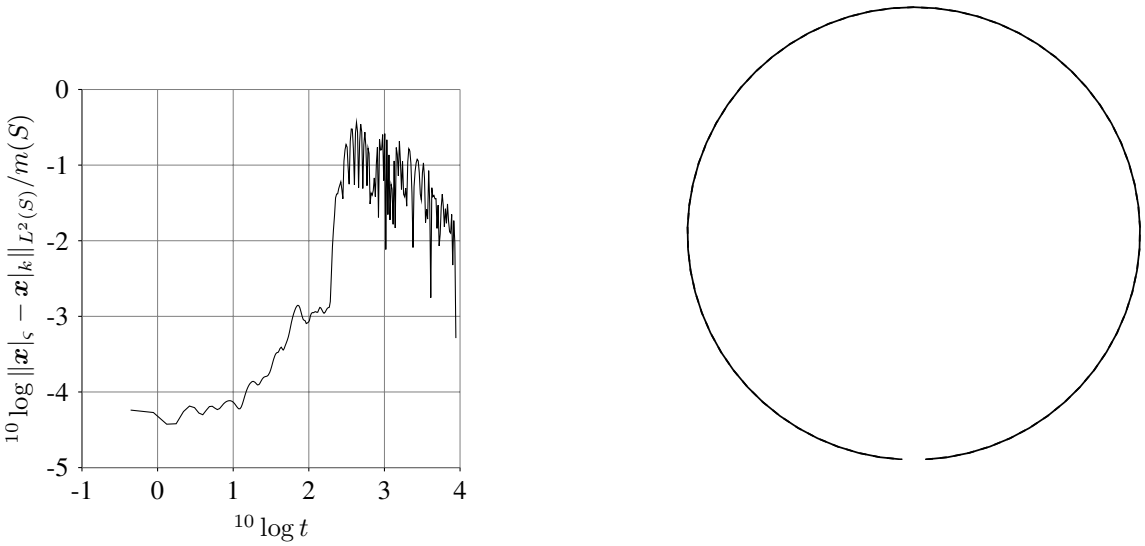

Figure 5: Left panel: time evolution of the difference between the structural response measured in the $L^2(S)$ norm. Right panel: steady state response, $\boldsymbol{x}|_k$ (solid), $\boldsymbol{x}|_\varsigma$ (dashed).

153 elements, refined where initial geometry requires this, as well as a time step of $6.5 \cdot 10^{-2}$, which are further subdivided as required to resolve the lubrication forces in the Stokes simulation. The results are presented in figure 7. Indeed, the effect of viscosity is more pronounced, causing the airbag to bulge and inflate very locally.

5 CONCLUSIONS

The FE/BE method is an enabling method within the realm of simulating inflatable structures, in view of the capability to handle large displacements and complex geometries. To assess this method, a planar setting is adopted in this paper. The corresponding mathematical modeling is discussed.

Two competing models are given for the structure, each attempting to mimic the behavior of the three-dimensional model. The first is a string of which the motion is restricted to the plane, the second is a cross section of a Kirchhoff-Love shell. It is seen that these models are identical up to linear terms. Numerical experiments confirm that these models indeed behave very similarly. The similarity of the response for the two structural models can be attributed to the fact that both models behave identically in the small-strain limit.

Also, a hierarchy of linear fluid models (viz., uniform pressure, potential flow and Stokes flow) is considered, and their behavior investigated. Two notable conclusions can be drawn. Firstly, it is observed that the potential flow model offers little advantage over uniform pressure in this context, as the numerical response is qualitatively identical. Secondly, and conversely, the commonly used uniform pressure model gives predictions that are both qualitatively and quantitatively different from the more refined Stokes model. We emphasize that this implies that FE/BE significantly enhances numerical simulations on complex folded domains with respect to the conventional uniform-pressure model, without the need to resort to volumetric meshing.

ACKNOWLEDGEMENTS

The authors would like to thank David Bourne for fruitful discussions. This research is supported by the Dutch Technology Foundation STW, which is part of the Netherlands Organization for Scientific Research (NWO) and partly funded by the Ministry of Economic Affairs, Agriculture and Innovation (project number 10476).

REFERENCES

[1] Antman, S.S.; *Nonlinear problems of elasticity*, Springer-Verlag, 1995.

[2] Bischoff, M.; Wall, W. A.; Bletzinger, K.-U.; Ramm, E.; *Models and Finite Elements for Thin-walled Structures*, in Encyclopedia of Computational Mechanics, volume 2, chapter 3 John Wiley & Sons, Ltd, 2004.

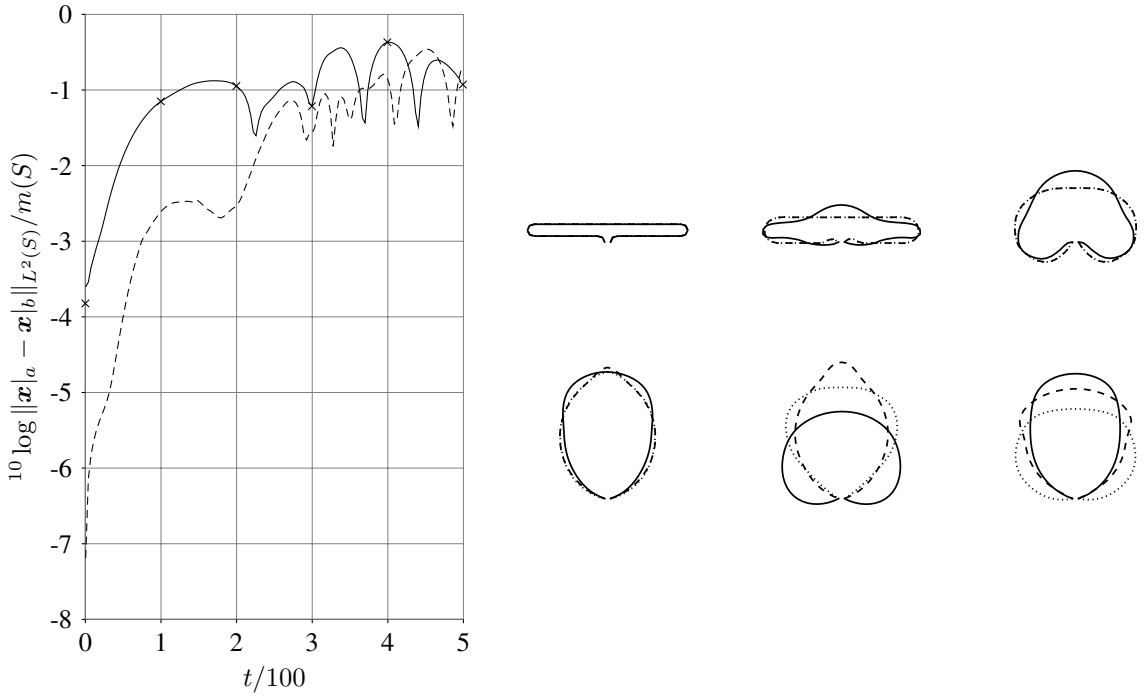

Figure 6: Left panel: time evolution of the difference between the structural responses measured in the $L^2(S)$ norm, $(a, b) = (s, p)$ (solid), $(a, b) = (p, u)$ (dashed). Right panel: snapshots of the response at the $\times$-marked time levels, $\boldsymbol{x}|_s$ (solid), $\boldsymbol{x}|_p$ (dashed), $\boldsymbol{x}|_u$ (dotted).

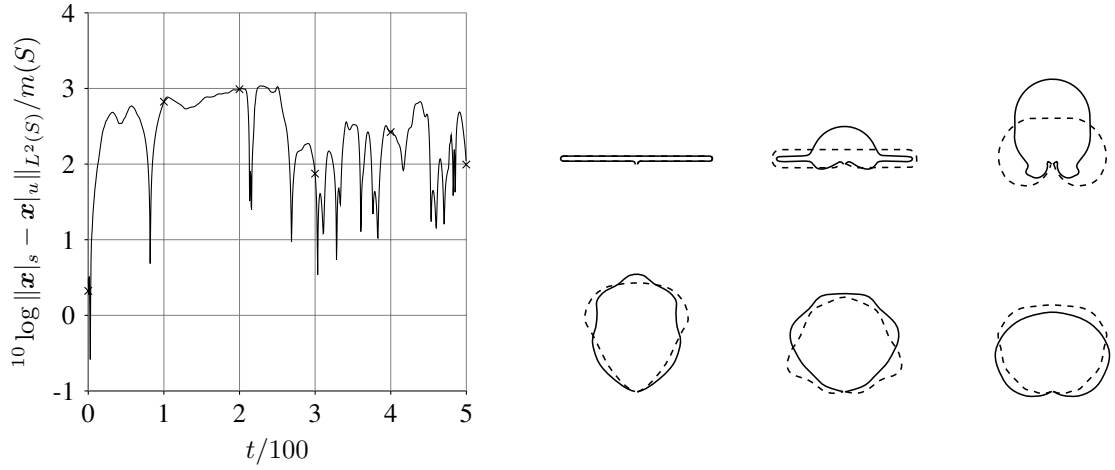

Figure 7: Left panel: time evolution of the difference between the structural responses measured in the $L^2(S)$ norm. Right panel: snapshots of the response at the $\times$-marked time levels, $\boldsymbol{x}|_s$ (solid), $\boldsymbol{x}|_u$ (dashed).

[3] Carstensen, C.; Stephan, E.P.; Adaptive coupling of boundary elements and finite elements, *Mathematical Modelling and numerical analysis*, **29**(7):779817, 1995.
[4] Cirak, F.; Radovitzky, R.; A LagrangianEulerian shellfluid coupling algorithm based on level sets, *Computers and Structures*, **83**:491498, 2005.
[5] Domínguez, C.; Stephan, E.P.; Maischak, M.; A FE-BE coupling for a fluid-structure interaction problem: Hierarchical a posteriori error estimates, *Numerical Methods for Partial Differential Equations*, 2011.
[6] Ern, A.; Guermond, J. L.; *Theory and practice of finite elements*, Springer, 2004.
[7] Anderson jr, J.D.; *Fundamentals of Aerodynamics*, McGraw Hill, 2001.
[8] Ladyzhenskaya, O.A.; *The Mathematical Theory of Viscous Incompressible Flows*, Gordon and Breach, 1963.
[9] Marklund, P.-O.; Nilsson, L.; Simulation of airbag inflation processes using a coupled fluid structure approach, *Computational Mechanics*, **29**(4-5):289297, 2002.
[10] Oden, J.T; *An Introduction to Mathematical Modeling: A Course in Mechanics* Wiley, 2011.
[11] Power, H.; Wrobel, L.C.; *Boundary Integral methods in Fluid Mechanics*, Computational Mechanics Publications, 1995.
[12] Opstal, van, T.M.; Brummelen, van, E.H.; A potential-flow BEM for large-displacement FSI, Technical Report 3-12 (`http://www.win.tue.nl/casa/research/casareports/2012.html`)
[13] Opstal, van, T.M.; Brummelen, van, E.H.; A Stokes BEM for large-displacement FSI, Technical Report 4-12 (`http://www.win.tue.nl/casa/research/casareports/2012.html`)
[14] Yong, D.; Strings, chains and ropes, *SIAM*, **48**(4):771781, 2006.
[15] Zienkiewicz, O.C.; Kelly, D.W.; Bettess, P.; The coupling of the finite element method and boundary solution procedures, *International Journal for Numerical Methods in Engineering*, **11**(2):355375, 1977.

The remainder of this page was intentionally left blank.